

Pinched Shells of Revolution: Experiments on High-Order FEM

H. Hakula*

J. Pitkäranta†

Abstract

Recent theoretical error estimates predict that high-order finite elements have the potential of overcoming a number of numerical difficulties associated with shell problems. In this work we support the error analysis by numerical experiments on thin, “pinched” shells of revolution loaded by two equal and opposite radial point loads. Different geometric categories of shells have strikingly different deformation properties under the same loading and kinematical constraints. This is illustrated by examples covering elliptic, parabolic, and hyperbolic shells. We demonstrate that elements of relatively high order (degree $p = 4\dots 6$), indeed, give quite accurate results as compared, e.g. with linear or quadratic elements which often lead to poor scale resolution and sometimes even to total failure. In a series of experiments we examine the impact of the degree p on a fixed problem for each shell category. In the hyperbolic case we also give a direct comparison between the traditional h -version and the p -version of FEM. The relative superiority of high-order methods in thin shells is confirmed by our results.

Key words: linear elasticity, shells.

AMS subject classifications: 65N30, 73C02.

1 Introduction

The aim of this paper is to demonstrate the effects of the shell geometry in linear shell problems and to advocate the use of high-order finite elements in these problems instead of using some special case-dependent “shell elements”.

*Harri.Hakula@hut.fi

†J.Pitkaranta@hut.fi

Institute of Mathematics, Helsinki University of Technology, Otakaari 1, 02150 Espoo, Finland

ICOSAHOM'95: Proceedings of the Third International Conference on Spectral and High Order Methods. ©1996 Houston Journal of Mathematics, University of Houston.

The approach we suggest here is that of standard finite elements of (sufficiently) high degree. How high the degree should be depends on the case, but normally it is in the range from 2 to 8. From the programming point of view this requires using the “ p -version” where the degree p is chosen by the user [13].

Admittedly, the high-order elements appear much more complicated than the traditional low-degree elements specially tuned for shells. However, raising the degree often has its advantages (at least within the standard FEM framework) as will be shown by the examples. In the practical diversity of shell problems induced by variations of geometry, load, and boundary conditions, high-order methods are in general more reliable (or “robust”) than low-order ones. In addition to this, in a given problem high-order methods often perform better with a given computing effort.

The basic source of numerical difficulties in shell problems is the small dimensionless parameter; the effective thickness of the shell, that appears e.g. in the energy formulation of the problem based on any classical dimension reduction model. The effective thickness is defined as $t = d/L$, where d is the actual thickness of the shell and L is the length scale one is trying to resolve with the numerical scheme; often the diameter but there are other possibilities as well [3].

Numerical difficulties arise when parameter t is small, i.e., when the shell is (effectively) thin. In fact, this must be assumed for the dimension reduction models to be valid. Why high-order methods are more reliable for thin shells may be seen from rather simple error analysis in the energy norm[3]. The result of this simplified analysis is easily stated: The relative error behaves as

$$(1) \quad \text{error} \sim K(t)(h/L)^p,$$

where h is the mesh spacing in the finite element scheme, p is the the degree of the elements, and $K(t)$ is a *locking factor* which may diverge as $t \rightarrow 0$. In the *worst* cases $K(t) \sim t^{-1}$, but there also are cases where the factor is not t -dependent, i.e., $K(t) \sim 1$. In the latter case, the finite

element scheme resolves the length scale under consideration as it should in the sense of approximation theory, i.e., optimally. Thus, there are cases where error amplification by factor $1/t$ (as compared with the best approximation) occurs in the finite element model and other cases where the numerical scale resolution is optimal.

The estimate (1) gives us an idea of when locking (as $t \rightarrow 0$) is most severe and how we should deal with it. The most dramatic failure of the finite element scheme is expected in cases where 1) the worst locking factor $1/t$ arises, and 2) the length scale to be resolved is large compared with the thickness of the shell, i.e., t is small. These worst features are joined in the so-called *membrane locking*. This occurs in the approximation of smooth, inextensional components of the displacement field; see [1], [10], [11]. Numerical locking in boundary layers is a more hidden effect, but it can also cause large errors in local quantities such as stress maxima.

In the model problems to be studied below, global inextensional deformations will be ruled out by the kinematical constraints, so the overall membrane locking is not a problem. However, locking can still occur in the resolution of the scales of the layers, since the worst locking factor $K(t) \sim t^{-1}$ in (1) occurs also here [3], and since the dominant layer scales are relatively wide (see [3]-[9], [11]).

Regarding what to do with locking, we can see from estimate (1) that when t is small but positive, raising p helps to narrow the gap in between the “best” and the “worst” cases and thus makes the finite element scheme more robust. Indeed, the estimate tells us that in order to achieve a given accuracy at given t and p , one needs in the “worst” cases mesh *overrefinement* by factor $\sim (1/t)^{\frac{1}{p}}$, as compared with the “best” cases. For example if $t = 0.01$, the overrefinement required at $p = 4$, say, is rather moderate as compared with that required at $p = 1$. Here is in fact the basic reasoning that suggests higher degrees in cases where locking is likely to occur in some relevant length scale.

In Chapter 2 we give the mathematical settings of the linear shell problem based on one of the familiar dimension reduction models. In Chapter 3 we present the results of a series of numerical experiments on the “pinched” shell problem, which is one of the well-known “obstacle-course” tests for numerical shell analysis [1]. Conclusions are drawn in Chapter 4.

2 The linear shell problem

In this work we study thin shells of revolution. They can formally be characterized as domains in \mathbb{R}^3 of the type

$$(2) \quad \Omega = \left\{ \underline{x} + z \underline{n}(\underline{x}) \mid \underline{x} \in \Gamma, -\frac{t}{2} < z < \frac{t}{2} \right\},$$

where $t \ll \text{diam}(\Omega)$ is the (constant) thickness of the shell, Γ is a surface of revolution defined as

$$(3) \quad \Gamma = \left\{ \underline{x} \in \mathbb{R}^3 \mid x_1 \in [-1, 1], x_2^2 + x_3^2 = \phi(x_1)^2, \right. \\ \left. \phi \in C^\infty[-1, 1], \phi > 0 \right\},$$

and $\underline{n}(\underline{x})$ is the unit normal to Γ . Here we have chosen the axial half-length of the shell to be the length unit. In the examples we set $t = 0.001$, so the shells to be studied are quite thin.

As is well known, there are three main categories of shell problems depending on the geometry of the mid-surface of the shell. For shells of revolution the different geometric categories can be defined in terms of the function ϕ in (3). The Gauss theory of surfaces states that at a given point a surface is called elliptic, parabolic, or hyperbolic, whether the Gauss curvature at that point is positive, zero, or negative; respectively. In the current setting, for a point $\underline{x} = (x_1, x_2, x_3)$, Γ is

[E] elliptic, if $\phi''(x_1) < 0$,

[P] parabolic, if $\phi''(x_1) = 0$, and,

[H] hyperbolic, if $\phi''(x_1) > 0$.

In the cases below it is assumed that for a given shell the condition holds on the whole interval $[-1, 1]$.

A shell is a three-dimensional body for which the standard 3D theory of elasticity can be considered accurate for small deformations. Here we consider one of the classical dimension reduction models which has gained popularity in finite element modeling. This model is similar to the Reissner-Mindlin model for plate bending and is sometimes named after Naghdi. In this model, the displacement field \underline{u} has five components u, v, w, θ, ψ , each a function defined over the mid-surface Γ . Here (u, v) and w are, respectively, the tangential and normal displacements of the mid-surface; and θ, ψ are the so called rotations.

We parametrize Γ with the usual axial/angular (principal curvature) coordinates so that $\Gamma = \{ \underline{\Psi}(x_1, x_2) \mid -1 < x_1 < 1, -\pi < x_2 \leq \pi \}$, where

$$(4) \quad \underline{\Psi}(x_1, x_2) = (x_1, \phi(x_1) \sin x_2, \phi(x_1) \cos x_2).$$

Then u, v, w are defined as the projections of the displacement on the directions

$$(5) \quad \underline{e}_1 = \frac{1}{A_1} \frac{\partial \underline{\Psi}}{\partial x_1}, \quad \underline{e}_2 = \frac{1}{A_2} \frac{\partial \underline{\Psi}}{\partial x_2}, \quad \underline{e}_3 = \underline{e}_1 \times \underline{e}_2,$$

respectively, where A_i are the so called Lamé parameters

$$(6) \quad A_1 = \sqrt{1 + \phi'(x_1)^2}, \quad A_2 = \phi(x_1),$$

and the rotations are defined by

$$(7) \quad \theta = \frac{1}{A_1} \frac{\partial w}{\partial x_1} - \frac{u}{R_1}, \quad \psi = \frac{1}{A_2} \frac{\partial w}{\partial x_2} - \frac{v}{R_2},$$

where further R_i are the principal radii of curvature defined as

$$(8) \quad R_1 = -A_1^3/A_2'', \quad R_2 = A_1 A_2.$$

Note that in the parabolic case $R_1 = \infty$.

Assume that the shell consists of homogeneous isotropic material with Young modulus E and Poisson ratio ν . Then the total energy of the shell in our dimension reduction model is expressed as

$$(9) \quad \mathcal{F}(\underline{u}) = \frac{1}{2} D [t a(\underline{u}, \underline{u}) + t^3 b(\underline{u}, \underline{u})] - q(\underline{u}),$$

where $D = E/(1 - \nu^2)$ is a scaling factor, $q(\underline{u})$ is the external load potential, and $a(\underline{u}, \underline{u})$ and $b(\underline{u}, \underline{u})$ represent the portions of total deformation energy that are stored in membrane and transverse shear deformations and bending deformations; respectively. The latter are quadratic forms independent of t and defined as

$$(10) \quad \begin{aligned} a(\underline{u}, \underline{u}) &= a_m(\underline{u}, \underline{u}) + a_s(\underline{u}, \underline{u}) \\ &= \int_{\omega} \left[\nu(\beta_{11} + \beta_{22})^2 + (1 - \nu) \sum_{i,j=1}^2 \beta_{ij}^2 \right] A_1 A_2 d\gamma \\ &\quad + \frac{1}{2} (1 - \nu) \alpha \int_{\omega} (\rho_1^2 + \rho_2^2) A_1 A_2 d\gamma, \end{aligned}$$

$$(11) \quad b(\underline{u}, \underline{u}) =$$

$$= \frac{1}{12} \int_{\omega} \left[\nu(\kappa_{11} + \kappa_{22})^2 + (1 - \nu) \sum_{i,j=1}^2 \kappa_{ij}^2 \right] A_1 A_2 d\gamma,$$

where β_{ij}, ρ_i , and κ_{ij} stand for the membrane, transverse shear, and bending strains, respectively and α is the so-called shear correction factor. We shall simply choose $\alpha = 1$. The strain-displacement relations are linear and involve, at most, first derivatives of the displacement components. For shells of revolution they can be expressed as

$$(12) \quad \beta_{11} = \frac{1}{A_1} \frac{\partial u}{\partial x_1} + \frac{w}{R_1},$$

$$(13) \quad \beta_{12} = \frac{1}{2} \left(\frac{1}{A_2} \frac{\partial u}{\partial x_2} + \frac{1}{A_1} \frac{\partial v}{\partial x_1} - \frac{v}{R_2} \frac{\partial A_2}{\partial x_1} \right),$$

$$(14) \quad \beta_{22} = \frac{1}{A_2} \frac{\partial u}{\partial x_1} + \frac{u}{R_2} \frac{\partial A_2}{\partial x_1} + \frac{w}{R_2},$$

$$(15) \quad \rho_1 = \frac{1}{A_1} \frac{\partial w}{\partial x_1} - \frac{u}{R_1} - \theta,$$

$$(16) \quad \rho_2 = \frac{1}{A_2} \frac{\partial w}{\partial x_2} - \frac{v}{R_2} - \psi,$$

$$(17) \quad \kappa_{11} = \frac{1}{A_1} \frac{\partial \theta}{\partial x_1},$$

$$(18) \quad \begin{aligned} \kappa_{12} &= \frac{1}{2} \left\{ \frac{1}{A_1} \frac{\partial \psi}{\partial x_1} + \frac{1}{A_2} \frac{\partial \theta}{\partial x_2} - \frac{1}{A_2} \frac{1}{R_2} \frac{\partial A_2}{\partial x_1} \frac{\partial w}{\partial x_2} \right. \\ &\quad - \frac{1}{A_2} \frac{1}{R_1} \frac{\partial u}{\partial x_2} - \frac{1}{A_1} \frac{1}{R_2} \frac{\partial v}{\partial x_1} \\ &\quad \left. + \frac{v}{R_2} \left(\frac{1}{R_2} \frac{\partial A_2}{\partial x_1} - \frac{1}{A_1^2} \frac{\partial A_1}{\partial x_1} \right) \right\}, \end{aligned}$$

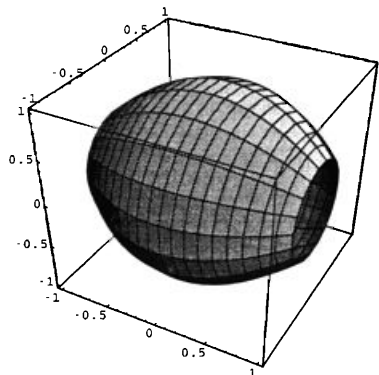
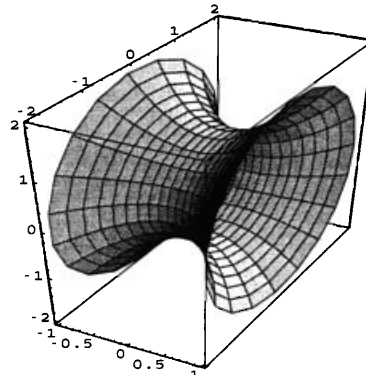
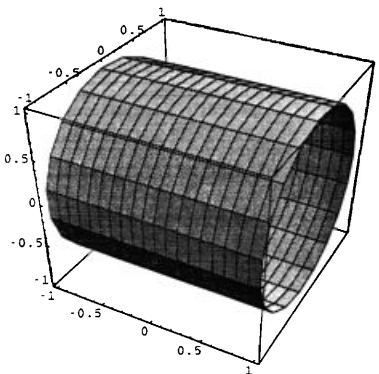
$$(19) \quad \kappa_{22} = \frac{1}{A_2} \frac{\partial \psi}{\partial x_2} + \frac{\theta}{R_2} \frac{\partial A_2}{\partial x_1}.$$

Within the above dimension reduction model, the exact displacement field is defined as the minimizer of the energy (9) under the assumed (homogeneous) kinematical constraints on $\partial \omega$. Finite element approximations can then be derived analogously applying the same energy principle. Indeed, since the strains involve only first derivatives of the displacement field, standard C^0 elements can be used. In this work we shall minimize the energy exactly as given by (9) through (11) without any numerical modifications. For further aspects of shell models and possible numerical tunings, the reader is referred to [11], [12] and the references therein.

As model problems we consider shells of revolution of the canonical type

$$(20) \quad \phi(x_1) = 1 + \xi x_1^2,$$

where $\xi \in (-1, \infty)$ is a parameter which determines the geometric category of the shell in question. In the numerical examples we choose $\xi = -\frac{1}{2}$ (elliptic), $\xi = 0$ (parabolic), or $\xi = 1$ (hyperbolic). A ‘‘pinched’’ loading is assumed where two radial point loads act on the opposite sides of the shell at $x = 0$. The same kinematical constraints are assumed

Figure 1: Elliptic: $\phi(x_1) = 1 - \frac{1}{2}x_1^2$.Figure 3: Hyperbolic: $\phi(x_1) = 1 + x_1^2$.Figure 2: Parabolic: $\phi(x_1) = 1$.

at both ends of the shell, so by symmetry the domain is reduced to the set

$$(21) \quad \omega = \{(x_1, x_2) \mid 0 < x_1 < 1, \quad 0 < x_2 < \pi/2\},$$

assuming that the point load is imposed at $x_1 = 0, x_2 = 0$. The load potential q in (9) is then $q(\underline{x}) = Q w(0, 0)$.

We shall look at the performance of standard finite element methods where each component of the displacement/rotation field is given the same finite element representation. This is based on triangular (cf. [13]) elements on ω of varying degree p . The underlying computer code [2], follows the standard p -version philosophy with hierarchic shape functions derived from orthogonal polynomials [13].

3 Numerical results

We present here results from numerical experiments on pinched shells. In Figs. (1), (2), and (3) we show the three

model shell geometries, each one representing one of the three categories defined in Chapter 2.

In the following we first compare the differences in deformation fields of the shells under the same loading. Having established the general setting we examine the effect of the degree p of the elements in each case separately. Finally, we compare the impact of the traditional method of decreasing h while using low-order elements in the hyperbolic case. The w -component of the displacement field is shown in the figures.

In all cases the loading and the computational domain are as described in Chapter 2. Additionally we define the Poisson ratio $\nu = 0.3$ and let $t = 0.001$. The kinematical constraints at $x = 1$ are $u = v = w = 0$. Unless otherwise stated, the mesh is a regular (aligned) 9×9 grid with 128 elements, diagonals moving from the bottom-left to the upper-right corner of ω . Thus the number of degrees of freedom varies depending on p as follows:

p	1	2	3	4	5	6
d.o.f	405	1445	3125	5445	8405	12005

Note that if the Koiter shell model with vanishing shear strains were assumed instead of the Reissner-Mindlin type model of Chapter 2, the transverse deflection under the load would be finite. In our case, however, the “exact” value $w(0, 0)$ is minus infinity.

3.1 Geometric categories

In Figs. (4), (5), and (6) we give a global visual comparison of the deformations at $p = 6$. It is evident, and also expected theoretically [4], [5], [9], that different geometries have clearly different profiles.

In the elliptic case the pinch-through can be seen from the “stacked” view. The contour plot (20 levels) is some-

what restless. Nevertheless, the deformations are concentrated in the vicinity of the load. The expected (dominant) scale of the range \sqrt{t} at the load is not well resolved due to the relatively coarse mesh. At $x = 1$, however, there is a trace of boundary layer.

In Fig. (5) we see the two dominant components of the displacement field in a parabolic shell. First, there is a very large local deformation in the vicinity of the load. Again, the largest deformations should appear in the range $\sim \sqrt{t}$ which is within the most deformed area. Secondly, there is a long-range damped oscillation in the angular direction. This is a predicted “layer” in the scale $\sim \sqrt[3]{t}$ [9]. In capturing this layer, it helps to have the mesh axially aligned as we have here (see [11]). The third possible layer at $x = 1$ is not visible at all.

Finally, in Fig. (6) we have a drastic departure from the two previous cases. There is a layer decaying transversally from the characteristic line emanating from the origin. The predicted scale is $\sim \sqrt[3]{t}$ [5], which is again well captured. Here the mesh diagonals help, since they are close to the characteristic line. The layer at $x = 1$ is also present in the picture.

3.2 Elliptic profiles (Figs. 7-10)

The deformations are all relatively small away from the load. As can be seen from Figs. (8), (9), and (10), at lower degrees of p there is some numerical oscillation. With higher p , we get smoother curves which has its impact when e.g. local stress maxima are computed. In Fig. (7) only the highest degree ($p = 6$) hints at slight bulging near the load. (The effect occurs within one element, so one cannot still be certain of the accuracy.)

3.3 Parabolic profiles (Figs. 11-14)

In the parabolic case the general trend is clear. Quadratic elements perform uniformly badly, whereas at $p = 4$ convergence is reached. Only at $x = 0$ is there any difference between $p = 4$ and $p = 6$. At $p = 3$ all features of the displacement field are captured, but the amplitudes of the maxima and minima are not obtained correctly.

3.4 Hyperbolic profiles (Figs. 15-18)

It appears that the hyperbolic case is the most challenging one. Again the convergence is met with $p = 4$. This time, however; $p = 3$ does not give acceptable results, thus wrecking the myth of $p = 3$ being all that one ever needs when dealing with shells.

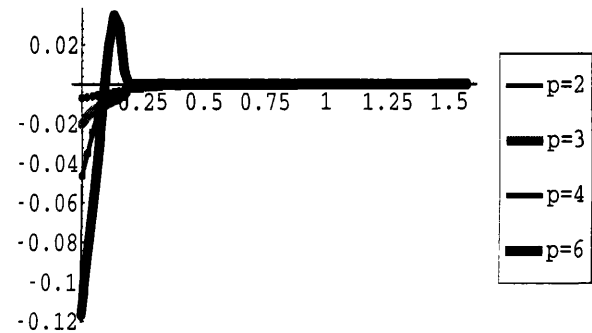


Figure 7: Elliptic: Profile of w at $x = 0$.

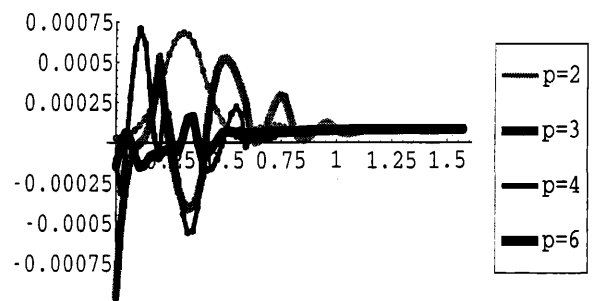


Figure 8: Elliptic: Profile of w at $x = 0.25$.

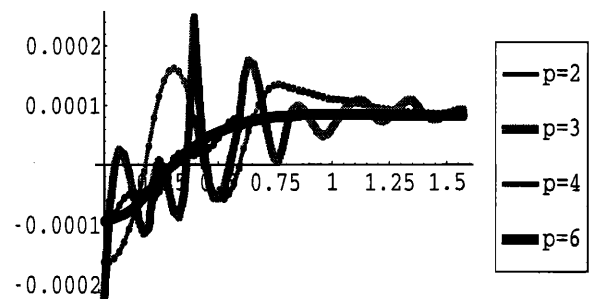
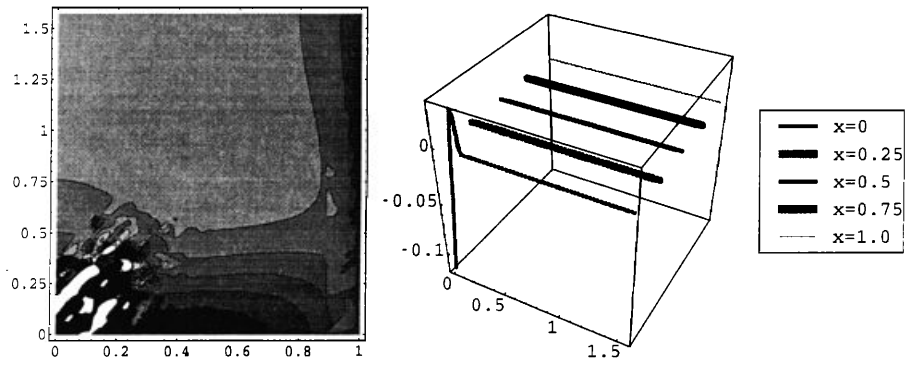
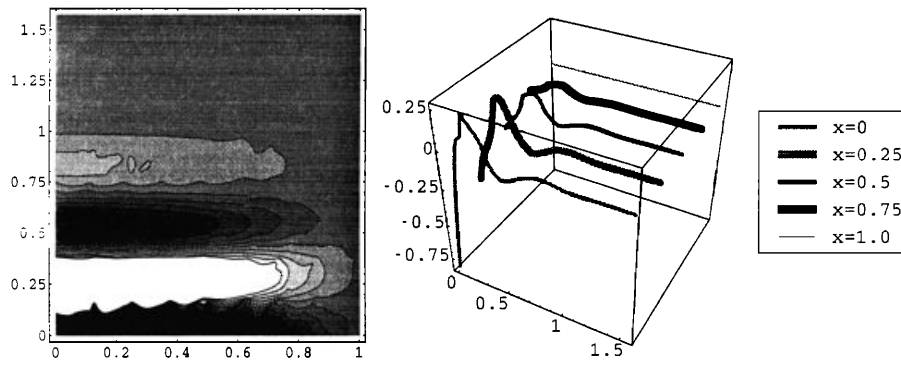
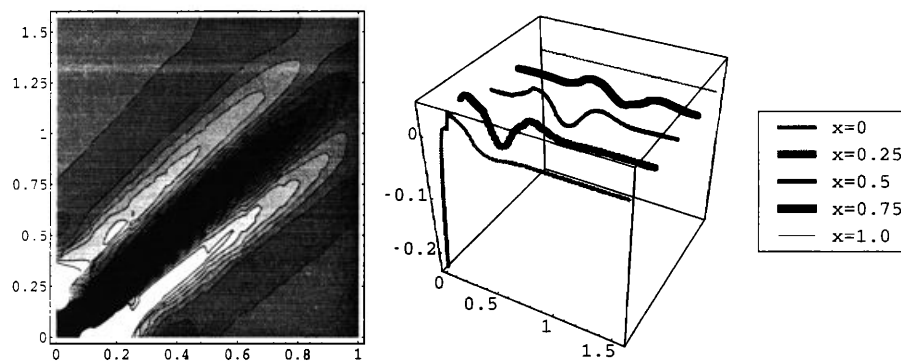


Figure 9: Elliptic: Profile of w at $x = 0.5$.

Figure 4: Elliptic: Overview ($p = 6$).Figure 5: Parabolic: Overview ($p = 6$).Figure 6: Hyperbolic: Overview ($p = 6$).

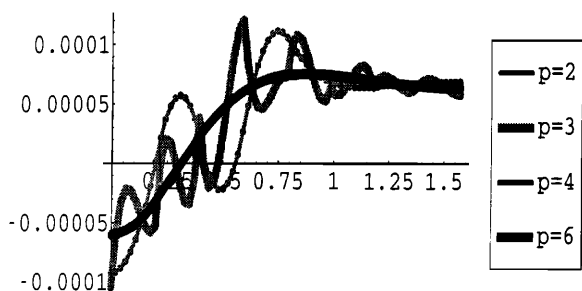


Figure 10: Elliptic: Profile of w at $x = 0.75$.

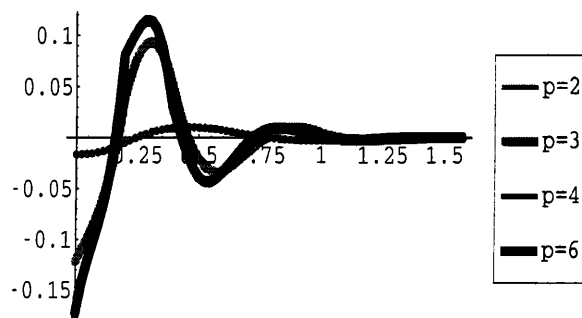


Figure 13: Parabolic: Profile of w at $x = 0.5$.

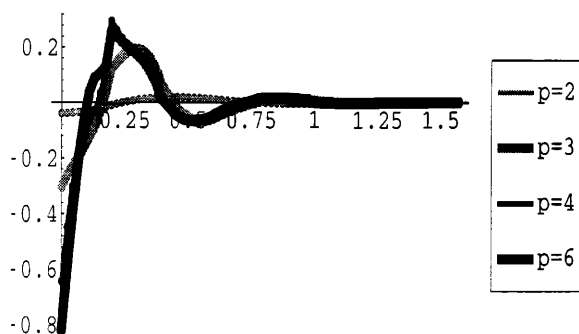


Figure 11: Parabolic: Profile of w at $x = 0$.

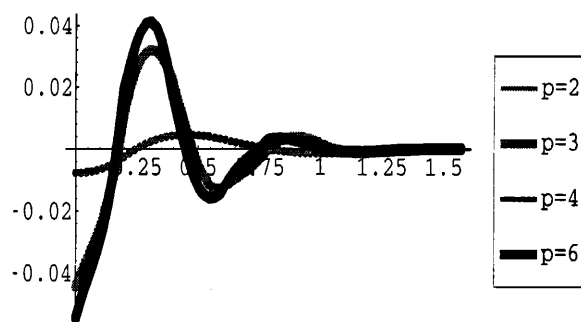


Figure 14: Parabolic: Profile of w at $x = 0.75$.

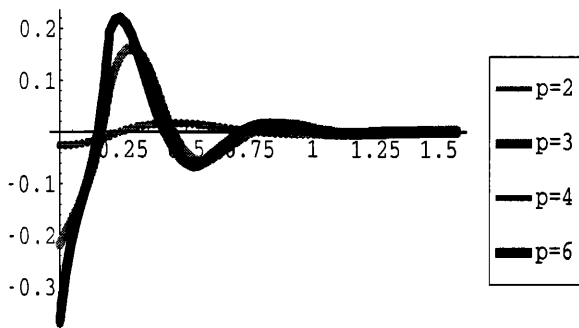


Figure 12: Parabolic: Profile of w at $x = 0.25$.

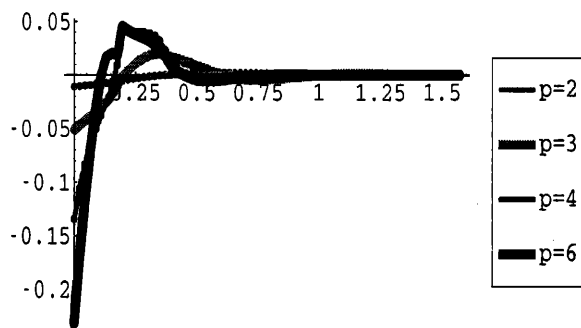


Figure 15: Hyperbolic: Profile of w at $x = 0$.

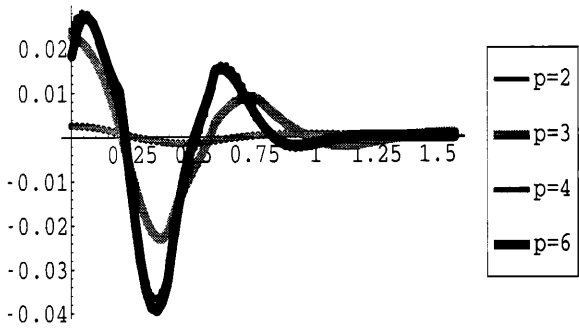


Figure 16: Hyperbolic: Profile of w at $x = 0.25$.

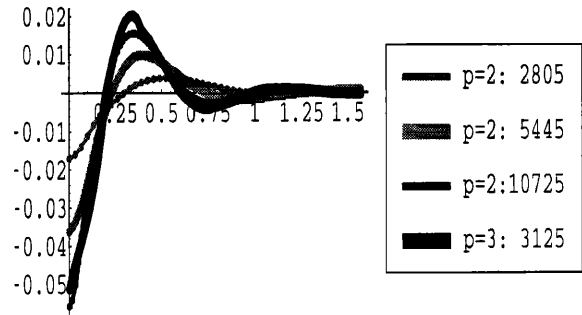


Figure 19: Hyperbolic: Comparison at $x = 0$.

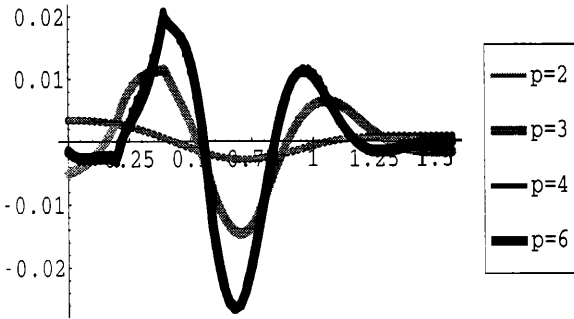


Figure 17: Hyperbolic: Profile of w at $x = 0.5$.

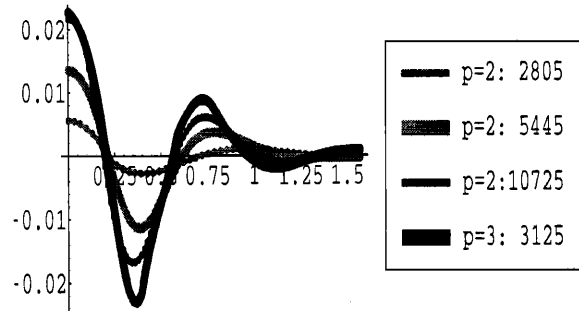


Figure 20: Hyperbolic: Comparison at $x = 0.25$.

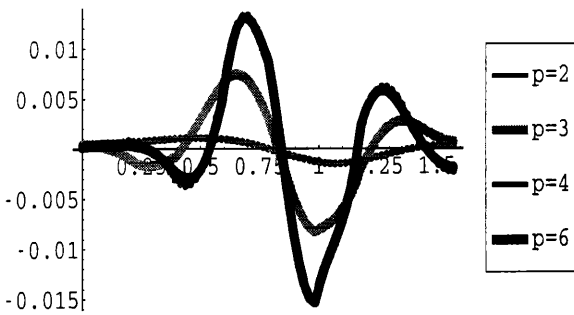


Figure 18: Hyperbolic: Profile of w at $x = 0.75$.

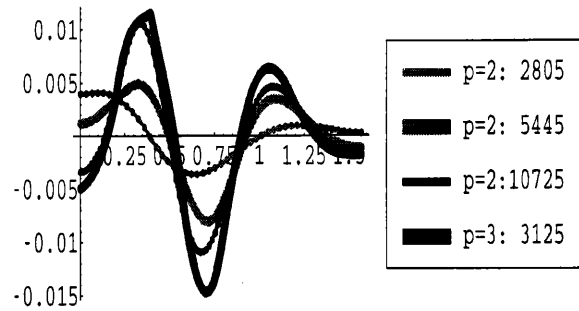


Figure 21: Hyperbolic: Comparison at $x = 0.5$.

3.5 h -version in hyperbolic case (Figs. 19 - 21)

Thus far we have examined the effect of varying p on a fixed mesh. In Figs. 19-21 we finally present results computed on finer grids with $p = 2$. The grids are regular: 9×17 , 17×17 , and 17×33 . We observe that even on the finest grid the low-order method does not compare with $p = 3$ on the coarser grid. (Note that the numbers of degrees of freedom are 10725 vs 3125.) Only at $x = 0$, the finer grid catches the pinch-through better. We should also recall that, as concluded earlier, $p = 3$ is not sufficient for this problem.

4 Conclusions

We have demonstrated with our experiments the benefits of using standard finite elements of high order in shell problems. The differences in the characteristic deformation fields of elliptic, parabolic, and hyperbolic shells have been shown as well. The connection between the characteristic lines and the deformation field is clear, especially in the hyperbolic case. In parabolic shells the axial lines play the same role. For elliptic shells, deformations are concentrated in the vicinity of the load.

The experiments confirm the theoretical result that raising the degree p reduces the need for mesh overrefinement needed to achieve a given accuracy for thin shells. It is evident that this effect depends only on the effective thickness and not on any other details of the problem. We have a consistent performance on all categories of shells of revolution.

In summary, we conclude that while staying within the standard finite element framework, raising the degree of the elements is a very effective way of improving the quality of numerical approximations to shell deformations. It is also a rather easy and natural way – when such an option in the program is available.

References

- [1] T. Belytschko, H. Stolarski, Wing Kam Liu, N. Carpenter and Jame S.-J. Ong: *Stress projection for membrane and shear locking in shell finite elements*, Comput. Methods in Appl. Mech. and Engrg. 51 (1985) 221-258.
- [2] H. Hakula: Licentiate Thesis, Helsinki University of Technology, to appear.
- [3] H. Hakula, Y. Leino and J. Pitkäranta: *Scale resolution, locking and high-order finite element modelling of shells*, to appear.
- [4] J. Piila: *Characterization of the membrane theory of a clamped shell. The elliptic case*, Math. Models and Meth. in Appl. Sci. (M³AS) 4 (1994) 147-177.
- [5] J. Piila: *Characterization of the membrane theory of a clamped shell. The hyperbolic case*, to appear.
- [6] J. Piila: *Energy estimates and asymptotic analysis in the theory of shells*, Doctoral thesis, Helsinki University of Technology, 1993.
- [7] J. Piila and J. Pitkäranta: *Energy estimates relating different linear elastic models of a cylindrical shell. (I) The membrane-dominated case*, SIAM J. Math. Anal. 24 (1993) 1-22.
- [8] J. Piila and J. Pitkäranta: *Energy estimates relating different linear elastic models of a cylindrical shell. (II) The case of a free boundary*, to appear in SIAM J. Math. Anal.
- [9] J. Piila and J. Pitkäranta: *Characterization of the membrane theory of a clamped shell. The parabolic case*, Math. Models and Meth. in Appl. Sci. (M³AS) 3 (1993) 417-442.
- [10] J. Pitkäranta: *The problem of membrane locking in finite element analysis of cylindrical shells*, Numer. Math. 61 (1992) 523-542.
- [11] J. Pitkäranta, Y. Leino, O. Ovaskainen and J. Piila: *Shell deformation states and the finite element method: A benchmark study of cylindrical shells*, Report A333(1994), Institute of Mathematics, Helsinki University of Technology.
- [12] J. Pitkäranta and M. Suri: *Design principles and error analysis of reduced-shear plate-bending finite elements*, to appear.
- [13] B. Szabo and I. Babuška : *Finite Element Analysis*, John Wiley & Sons, 1991

